Vol. 44, No. 2 (2022) 268-282, DOI: 10.24874/ti.1168.08.21.11

Tribology in Industry

www.tribology.rs

RESEARCH

Analysis of Oil Distribution and Reduction of Axial Force due to Oil Supply in a Multi-Plate Clutch

Daniel Groetsch[a,*], Rudi Motzet[a], Katharina Voelkel[a], Hermann Pflaum[a], Karsten Stahl[a]

[a]Gear Research Centre (FZG), Technical University of Munich, 85748 Garching, Germany.

Keywords:

Wet clutch
Sealed clutch
Clutch simulation
Reduced pressure
Pressurized oil supply
Oil distribution
Constant slip
Limited slip
Oil distributor design
Oil supply design
Computational fluid dynamics (CFD)

* Corresponding author:

Daniel Groetsch
E-mail: daniel.groetsch@tum.de

Received: 16 August 2021
Revised: 20 October 2021
Accepted: 11 November 2021

A B S T R A C T

Wet multi-plate clutches enable safety-critical operations in various types of powertrains. Ensuring sufficient oil coverage on each friction interface of industrial clutches is achieved by pressurized oil supply. The challenge of building capable test rigs to study oil and pressure distribution inside a practically relevant loaded clutch and the limited availability of test parts due to small batch sizes determine the demand for numerical studies. This contribution presents results obtained by experimentation on a component test rig and by numerical studies with computational fluid mechanics of a wet industrial clutch. A transient moving mesh approach with a laminar, incompressible, and isothermal flow model is applied to the fluid domain representing the test rig setup. The investigations are validated by comparing pressure measurements with simulation results. The influences of varying operating conditions (oil flow, speed) and geometry of oil supply in the inner carrier on the oil and pressure distributions are analyzed. Regardless of operating conditions or geometrical variations of the inner carrier, a nearly uniform oil supply to all friction interfaces is achieved. The hydraulic oil pressure lowers the effective axial force at the friction interfaces, and therefore reduces torque transfer capacity up to 29%, depending on operating conditions.

1. INTRODUCTION

Typical use cases for wet multi-plate clutches include the acceleration of large propeller and generator masses in a secure manner in the marine industry, or comparable heavy-duty applications in other industrial and agricultural powertrains. These applications require clutches with high torque and high heat capacity. The clutch torque can be calculated from the coefficient of friction (CoF) (μ), pressure (p), and the clutch geometry (gross friction surface A_f, mean friction radius r_m, and number of friction interfaces z) according to formula (1).

$$T_f = \mu \cdot p \cdot A_f \cdot r_m \cdot z \quad (1)$$

The reliability (a.o. [1–3]) and shifting quality [4] of wet clutches are notably influenced by thermal loads during operation. Due to the typical small batch sizes of industrial clutch systems, there is limited capability for functionality and durability tests on prototype parts. Thus, there is ongoing

research in mathematical modeling of the thermal behavior and oil distribution of wet multi-plate clutches (a.o. [5–7]). The spatial resolution ranges from real-time capable one-dimensional solutions [4, 7], to two- and three-dimensional calculation domains (a.o. [5, 6, 8, 9]). The calculation domains for thermal simulations typically solve the temperature profile of one friction interface, denoted as the thermal critical, as well as half of the connected carrier and steel plates [6, 8, 10]. Calculation times can be reduced by assuming complete [6] or partial angular symmetry [8, 10]. However, some approaches solve the temperature fields of the entire clutch, including all plates [9, 11]. This allows studying of the effects of reduced normal force at each friction interface, due to friction in connecting splines or hydrodynamic pressure [2, 9]. [9] shows that the second interface is usually severely thermally loaded in their numerical studies with twelve friction interfaces. However, these findings lack validation from comparison with experimental results.

The oil flow defines cooling conditions within the clutch and is therefore an important part of thermal models. Solving the two-phase-flow of oil-air mixtures at the friction interfaces is computationally expensive (a.o. [10–12]). However, the pressurized oil supply in heavy-duty applications ensures single-phase flow within a wide range of operations, thus maximizing the heat transfer coefficient as experimental and analytical investigations confirm [13]. Recent publications show that CFD simulations enable the estimation of oil distribution at each friction interface depending on loads and oil distributor patterns [11, 12]. Even the calculation of conjugate heat transfer coefficients between oil flow and solid regions depending on groove patterns and applied loads [10] seems to be possible. According to [10], the right choice of rotational direction and an appropriate choice of groove angle can increase conjugate heat transfer coefficients in a disengaged automotive clutch by five times. The influence of the pattern of oil distributors at the inner carrier is studied by [11, 12] and shows nonlinear effects on oil distribution at each friction interface. Even six evenly distributed oil inlets lead to non-uniform oil distributions [11], which corresponds to the experimental investigations of [14]. The authors state that the design of the inner carrier dominates oil distribution at the friction interfaces [14]. In contrast to results in this publication, these investigations are based on automotive / motorcycle clutch designs without pressurized oil supply. Another approach is to simplify the oil flow by means of the homogenized Reynolds equation [8] or by solving a simplified 1D model [6]. This significantly reduces computational costs, but prohibits oil distribution analysis and introduces new input parameters that have to be gathered by preliminary simulations [8] or measurements [6, 8].

Clutches operate in the open and closed modes, whereas heating only takes place during sliding phases under axial force. In the open and closed modes, the clutch is cooled by oil flow. Most CFD publications focus on the open mode and the calculation of cooling performance and drag torque (a.o. [15–17]). However, few models consider the closed state that is solved stationary (a.o. [8, 10, 11]) or transient (a.o. [9]) (constant sliding velocity). The calculation of shifting cycles [6] with long durations involves transitions between open and closed modes, and could be important for designing clutches that are operated in both regimes. However, constant slip is a typical mode of operation in industrial / marine powertrains and limited slip differentials in automotive gearboxes.

Calculation models should be validated by benchmarking with measurements from test rigs or practical applications. A typical approach to validating thermal models is to compare calculated temperatures at a specific location with signals from thermocouples (a.o. [6–8, 10, 18]). Validation of complex fluid simulations is achieved by correlating visual investigations of the plates after test rig runs [12], or by designing special test rigs capable of high speed camera recordings [11], particle-image-velocimetry [19], fluorescence based investigations [20], or neutron-imaging methods [14]. However, depending on the test rig setup, real life operating conditions with parts from serial production are often impossible to investigate. Besides the time and effort required to prepare these complex setups, they also require replacement of plate materials (and manufacturing processes) e.g. with sapphire [20], plastics [11], or aluminum [14], to enable the taking of measurements. The limited significance of the results for real life applications should therefore be considered [19].

There seem to be nearly no published results available about the pressure and oil distribution in an activated wet multi-plate clutch operated in constant slip. This paper therefore aims to extend

the knowledge of oil and pressure distribution in a typical industrial wet clutch with pressurized oil feeding.

We analyze the oil distribution per friction interface, the interaction of static oil pressure and applied axial force on the clutch, and how these findings are influenced by the pattern of the oil distributor of the inner carrier. The results should thus enable the improvement of oil models for heat calculations and can be used as guidelines for the design of oil distributor patterns for similar clutches.

2. RESEARCH METHOD

2.1. Experimental Investigations

The experimental investigations were carried out on the ZF / FZG KLP-260 wet brake component test rig. The description of the test rig is according to [21, 22]. The test rig operates in brake mode where the outer carrier is fixed and the inner carrier rotates as pictured in Fig. 1.

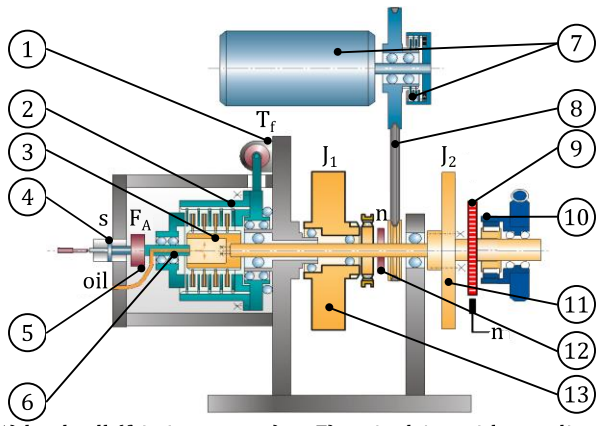

1) load cell (friction torque)
2) outer carrier
3) inner carrier
4) hydraulic piston
5) load cell (axial force)
6) oil injection
7) main drive with coupling
8) belt drive
9) incremental encoder
10) creep drive
11) adjustable flywheels
12) tachometer
13) switchable flywheel

Fig. 1. Test rig ZF/FZG KLP-260 – schematic sketch according to [21].

The test rig enables the mounting of a complete clutch package of a gearbox with the corresponding carriers. The inner plates are placed on the inner carrier which is installed on the inner shaft and connected to the fly wheels (J1, J2). The friction work of the clutch can be adjusted through variable installations of fly wheels J_1 as well as by engagement of the basic inertia J_2.

The pressure is applied on the outer plates by a force controlled hydraulic piston. The friction torque is measured at the outer carrier. Cooling oil can be supplied centrally into the inner carrier, externally from the top of the housing or by oil sump. The oil flow rate and the thermostat-controlled feeding temperature can be adjusted in a wide range. For brake engagement tests, the main shaft with the inner carrier and the fly wheels are accelerated by the speed-controlled main drive to a defined differential speed Δn. During the engagement process, the main drive and the inner shaft are decoupled through an electromagnetic coupling. In creeping conditions and in constant slip mode a defined axial force is applied on the clutch plates. The creep or main drive then accelerate the clutch to a defined slip speed. The rotational speed in low speed creep and slip modes is measured with high resolution by an incremental encoder. Table 1 summarizes the technical data of the test rig.

Table 1. Technical data of test rig ZF/FZG KLP-260.

Variable small fly wheels	J_1 = 0.12 ... 0.75 kgm^2
Basic inertia	J_2 = 1.0 kgm^2
Plate diameters	d = 75 ... 260 mm
Max. torque	$T_{f,max}$ = 2000 Nm
Differential speed	Δn = 0 ... 7000 min^{-1}
Slip speed	Δn = 0...140 min^{-1} (creep drive) Δn = 0...7000 min^{-1} (main drive)
Torque in slip mode	$T_{f,slip,max}$ = 2000 Nm (creep drive) $T_{f,slip,max}$ = 60 Nm (main drive)
Max. axial force	F_A = 40 kN
Feeding oil temperature	ϑ_{oil} = 30 ... 150 °C
Feeding oil flow rate	$\dot{v}_{Oil}$ = 0 ... 7 l/min
Feeding oil pressure	0 ... 6 bar

We extended the measurement accuracy table of the test rig published in [22] by analyzing the uncertainty of the installed oil pressure sensor by taking into account the findings of Baumgartner [23]. She applied the rules of the Guide to the Expression of Uncertainty in Measurement (GUM) [24] and DIN EN ISO 14253-2 [25] to the KLP-260 test rig. Furthermore, we estimated the offset of the thermocouples at 0 °C from the norm curve by calibration of the test rig setup with distilled ice water.

Table 2 summarizes the extended version of measurement accuracy for the FZG / KLP-260 test rig.

Table 2. Overview of measurement accuracy on the ZF / FZG KLP-260 test rig (confidence level 95 %) extended version acc. to [22].

Measured variable	Uncertainty
Axial force	+/- 1.3 %
Torque	+/- 0.4 %
CoF	+/- 1.3 %
Speed (main engine)	+/- 0.2 %
Speed (creep engine)	+/- 0.9 %
Thermocouple type K class 1	+/- 1.8 K (DIN) / +/- 0.3 K (estimate from calibration)
Feeding oil pressure	+/- 0.1 bar

For our numerical and experimental studies, we used steel (outer) and friction (inner) plates from serial production of an industrial application. Fig. 2 shows the waffle groove pattern on the sinter friction interface of the inner plates and the design of the steel plates.

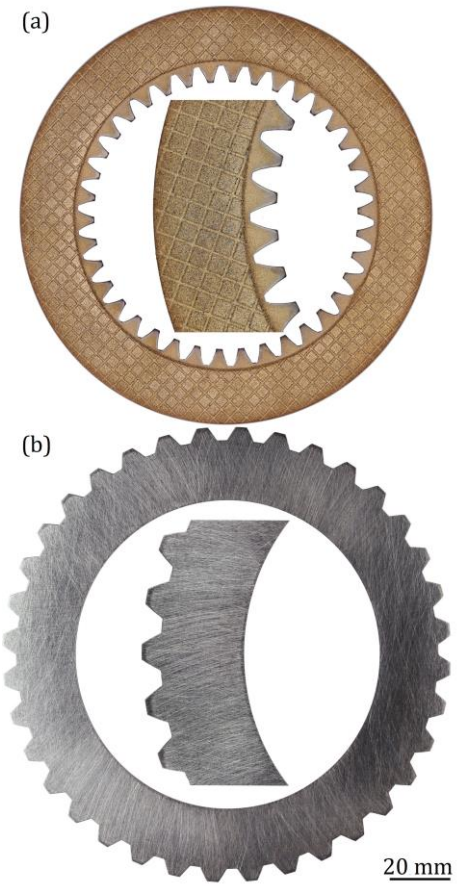

Fig. 2. (a) Friction plate (fp) and (b) steel plate (sp).

We used a clutch package with four (dynamic operations, Fig. 3 (a)) and eight (static operations, Fig. 3 (b)) friction interfaces. The mean diameter of the clutch is $d_m = 123$ mm. Further details on the geometric parameters and materials are summarized inTable 3.

Table 3. Summary of geometric parameters and materials of clutch D122.

Identifier	D122		
Part	Steel plate	Friction lining	Carrier plate
Inner diameter /mm	102	104	95.3
Outer diameter /mm	147	141	141
Thickness /mm	3	0.68	2.3
Material	Steel	Sinter	Steel

We measured temperatures in the first (hydraulic piston side), middle, and last (drive side) steel plates with a thermocouple (NiCrNi Type K Class 1, ⌀ 0.5 mm, response time approx. 30 ms calculated acc. to [26]), as pictured in Fig. 3. We applied a high-density polysynthetic silver thermal compound on the thermocouples and placed them in a circumferential drill hole (⌀ 0.6 mm) positioned at approx. 12 o´clock in the midplane of the steel plates with a drill depth of approx. the mean radius.

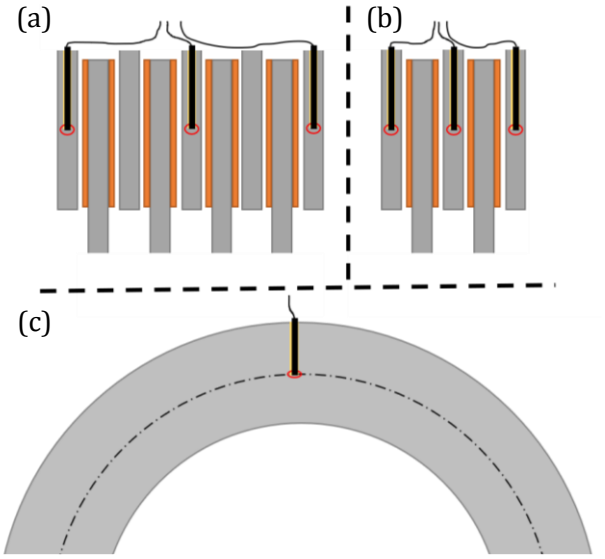

Fig. 3. Positioning of the thermocouples during (a) static operations, (b) dynamic operations and (c) the circumferential positioning.

Table 4 summarizes technical data obtained from the data sheet of the lubricant that was used for all tests and simulations. Density and

viscosity properties for temperatures not listed in the table are calculated acc. to DIN-51757 [27] and DIN-51563 [28].

Table 4. Technical data of lubricant.

	Density 15 °C	Kin. visc. 40 °C	Kin. visc. 100 °C
L-301	891 kg/m^3	100 mm^2/s	11.4 mm^2/s

The test procedure is split into static and dynamic operations. Static operations are performed with a clutch package consisting of five steel plates and four friction plates, therefore eight friction interfaces. In dynamic operations, the clutch size is reduced to four friction interfaces, due to torque limitations of the main drive during constant slip operations (see Table 1).

All experimental tests are performed with parts after 3,000 running-in cycles (cycle time 15s) have been conducted [29] (see Table 6).

As summarized in Table 5, we varied the oil injection temperature and the oil flow rate during static operations.

The load stages during running-in and in dynamic operation mode (constant slip) are summarized in Table 6. We varied oil flow rates and differential speeds. In our numerical study, the ratio of rotational speed between steel and friction plates was varied as well. Cycle time during dynamic operations is 900 s whereas it is a few seconds during static operations to ensure that steady state conditions for temperature and pressure signals are reached.

The nominal pressure is held constant at 0.75 N/mm^2 during static operations and 0.2 N/mm^2 during dynamic operations. All specific values are normalized by gross friction surface area (A). The load stages cover typical working conditions of the clutch in real world applications.

Table 5. Operating conditions during static operations (ST).

	Specific flow rate / mm^3/mm^{2}s	Oil temperature / °C
ST1	0.5	40 / 60
ST2	1	40 / 60
ST3	1.5	40 / 60
ST4	2	40 / 60

Table 6. Load stages during running-in (E) and in constant slip (LS - dynamic operations).

	Specific flow rate / mm^3/mm^{2}s	Sliding velocity $v_{s,mean}$ / m/s	Ratio n_{sp}/n_{fp}
E	1.25	10	0
LS1	0.75 / 1.5 / 2.5	2.5	0
LS2	0.75 / 1.5 / 2.5	5	0
LS3	0.75 / 1.5 / 2.5	7.5	0
LS4	0.75 / 1.5 / 2.5	10	0
LS5*	2.5	5	0.5
LS6*	2.5	0	1.0
*numerical study			

In the test rig, we can define and measure the speed of the inner carrier, oil flow rate, oil injection temperature, and clutch pressure (hydraulic piston). Additionally, we measure the transferred clutch torque, steel plate temperatures, and the oil pressure near the oil injection nozzle. Fig. 4 shows recorded data during static operations (variant I, L-301, ϑoil = 40 °C, static operation ST1). As we are interested in steady state conditions the evaluation interval is chosen such that the pressure and temperature signals are nearly constant. Within this interval we calculate the median and the 2.5th and 97.5th percentile from the continuous signals.

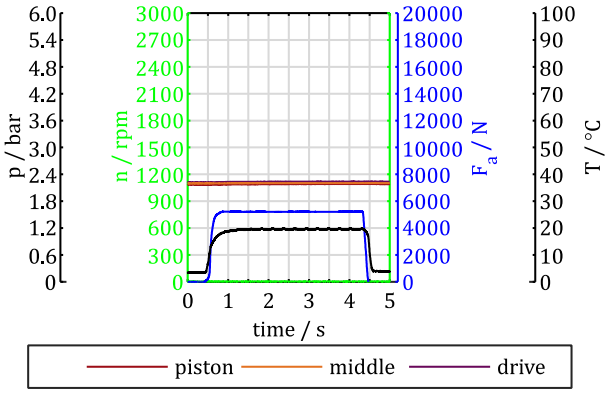

Fig. 4. Recorded signals differential speed (green), axial force (blue), oil pressure (black) and thermocouples (red, orange, purple) from test rig, (variant I, L-301, ϑ_{oil} = 40 °C, static operation ST1).

2.2. CFD Approach

The calculation domain of our CFD approach represents the clutch setup in the test rig that is shown in Fig. 5. The outer carrier is fixed to the housing of the test rig. The inner carrier is engaged with the main drive via the test rig

shaft. The axial force is applied on the steel plates by a force controlled hydraulic piston. The lubricant is supplied to the inner carrier region by the oil injection nozzle. The lubricant is then distributed to the clutch package through the radial holes in the inner carrier.

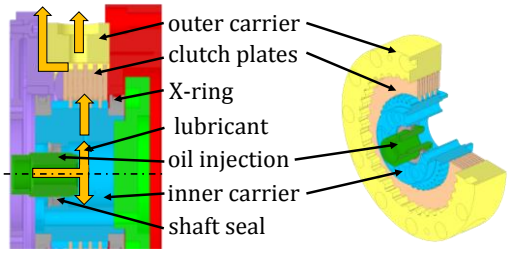

Fig. 5. Test rig setup of multi-plate clutch.

There are two variants of the pattern of the oil supply through the inner carrier, since recent publications see the main influence on oil distribution to be the inner carrier design [11, 12, 14]. Fig. 6 visualizes the difference between the two variants. The axial spacing of the holes for both variants ensures oil supply at each friction interface. The circumferential spacing varies, since variant I supplies fresh oil at every axial position within a third of a turn, and variant II within one turn of the inner carrier.

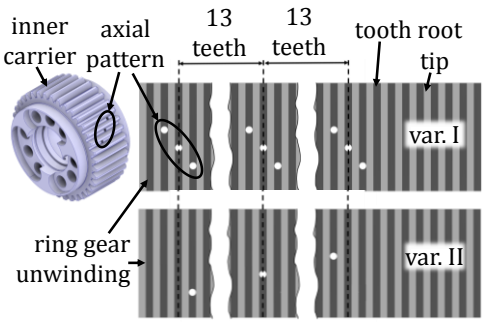

Fig. 6. Oil distributor variants of the inner carrier.

After passing the waffle grooves (in the plate-area), the oil leaves the axial and radial clutch package at the outer carrier. Two X-rings and a shaft seal ensure that the fluid passes the grooves during static and dynamic operations. Therefore, with sufficient oil supply we expect a single-phase oil flow. The pattern of oil supply holes in the inner carrier can be varied by the use of grub screws.

Fig. 7 shows the boundaries of our calculation domain for the static case with eight friction interfaces and the naming of the mesh regions. Four regions can be distinguished. The inlet-area contains fluid regions of the oil supply nozzle and the inner carrier as far as the end of the radial holes. The inner carrier-area is made up of the splines between the inner carrier and the clutch plates. Furthermore, the plate-area represents the grooves of the friction plates. The outer carrier-area is derived from the splines between the clutch plates and the outer carrier.

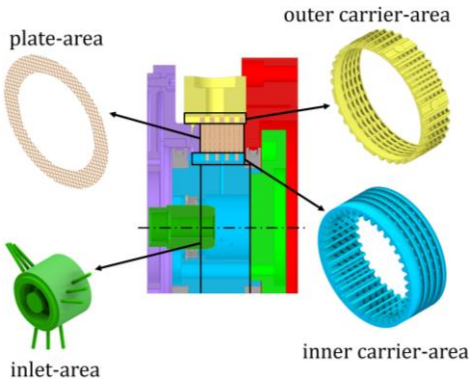

Fig. 7. Regions of calculation domain (boundaries marked with black lines).

The CFD model for the calculation of the oil and pressure distribution is developed in the SimericsMP+ commercial software v5.0.15 [30].

The flow is modeled as laminar, incompressible, and isothermal. These assumptions are based on a Reynolds criteria, prior publications, and experimental investigations.

The Reynolds number (*Re*) is calculated by dividing a characteristic flow velocity *u* and length scale *d* by the kinematic viscosity *ν* (see formula (2)) [26].

$$Re = \frac{u \cdot d}{\nu} \tag{2}$$

According to [31], the flow inside the grooves can be characterized by the rotational (*u*: rotational velocity of the plate at inner diameter) or average flow (*u*: average flow velocity through grooves) Reynolds numbers with the groove width as the characteristic length scale *d*.

We assume that circulation of the flow inside the grooves (more details in [18]) is dominated by the main eddy and thus small scale turbulence effects can be neglected [31].

Modeling the oil flow through a grooved clutch as laminar pipe flow [32–34] also suggests a laminar flow in the groove region. The calculation of the Reynolds number for the pipe flow model uses the average flow velocity as characteristic velocity, but the characteristic length scale is defined as the

spare hydraulic diameter calculated by the division of cross section area (A_{groove}) and length of the contour (c_{groove}) of the groove (see formula (3)).

$$d_{spare,hydraulic} = 4 \cdot \frac{A_{groove}}{C_{groove}} \quad (3)$$

The summary of calculated Reynolds numbers for severe operating conditions in our study and the limits for transition to turbulent flow regimes in Table 7 show that the laminar assumption is valid to the best of our knowledge.

Table 7. Calculated Reynolds numbers and laminar limits for ν = 11,4 mm^2/s and $v_{s,mean}$ = 10 m/s.

	Value	LAMINAR limit
$Re_{avg,Payvar}$	77	Typical below 500 [31]
$Re_{avg,Payvar}$	645	1,800* [31]
$Re_{avg,Pfleger,Haemmerl,Wohlleber}$	28	<< 2,300 [32–34]
*Authors use a laminar model for flow with Re = 1,800 and show good agreement with the measurements		

If the clutch operates long enough in constant slip, measurements show that the plate temperatures are nearly constant [18]. Considering the small cross section of the grooves and therefore the small volume of oil that must be heated, it seems justifiable to assume an isothermal flow. The motivation for the assumption is the trade-off to reduce computational effort and modeling complexity, while accurately enough representing the physics.

Although we assume steady conditions regarding oil heating in the grooves, the flow is solved as unsteady to capture the effects of the rotating oil distributor holes in the inner carrier.

We use the flow module with dynamic mesh motion to solve the continuity (see formula (4)) and momentum (see formula (5)) equations on an arbitrary control volume ($\Omega(t)$), whose boundary ($\sigma(t)$) is moving with the grid velocity V_g (flow velocity V).

$$\frac{\partial}{\partial t}\int_{\Omega(t)} \rho \, d\Omega + \oint_{\sigma} \rho\left(\vec{V} - \vec{V}_g\right) \cdot \vec{n} \, d\sigma = \int_{\Omega(t)} S_m \, d\Omega \quad (4)$$

$$\frac{\partial}{\partial t}\int_{\Omega(t)} \rho\vec{V} \, d\Omega + \oint_{\sigma} \rho\left[\left(\vec{V} - \vec{V}_g\right) \cdot \vec{n}\right]\vec{V} \, d\sigma = \oint_{\sigma} (\bar{\tau} \cdot \vec{n}) \, d\sigma - \oint_{\sigma} p\vec{n} \, d\sigma + \int_{\Omega(t)} \rho\overrightarrow{B_f} \, d\Omega + \int_{\Omega(t)} \vec{F} \, d\Omega \quad (5)$$

Further details can be found in the software documentation [30].

The CFD solver is based on the finite volume method and a pressure-based solver. We use upwind interpolation for the pressure solver, and second order upwind for the velocity solver. The algebraic multi-grid method is used to solve the pressure equations, and the conjugate gradient squared method is applied to the velocity equations.

Fig. 8 shows the calculation domain for variant I with highlighted in- and outlet areas. At the inlet, we specify the oil flow according to the test conditions (see Table 5, Table 6). The outlets are set to an ambient pressure of 0 bar.

In static operation modes, the remaining walls of the calculation domain are set to stationary solid walls. For the dynamic operation modes (constant slip), the components adjacent to the calculation domain are divided into input and output sides. Components of the input side have the rotational speed of the drive; components of the output side have the rotational speed of the outer carrier of the clutch.

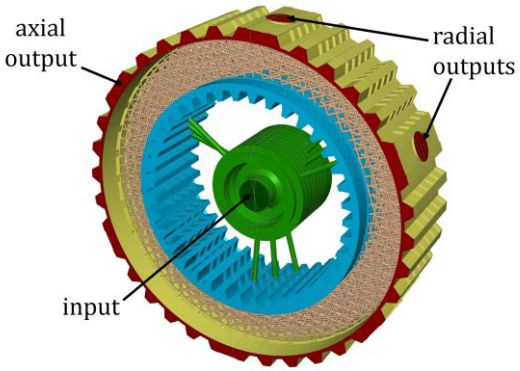

Fig. 8. Calculation domain variant I with marked in- and outputs.

The computational mesh is created by using the implemented body-fitted binary three-mesh algorithm, which produces a highly efficient hexagonal dominated mesh (a.o. [35]). A preliminary mesh study showed that a mesh size with a relative maximum cell size of 0.005 is an optimal trade-off in terms of computational effort and quality of results. Therefore, three different meshes with different cells were used, as summarized in Table 8.

Table 8. Cell properties in preliminary mesh study.

Mesh type	Relative maximum cell size	No. of cells.
Rough	0.01 (0.002)*	10 Mio.
Standard	0.005 (0.002)*	12 Mio
Fine	0.002 (0.001)*	20 Mio
*Refinement zones		

The so called rough, standard, and fine meshes differ in cell size and total number of cells. The meshes have three refinement zones (RZ I – III) to resolve oil shear and large velocity gradients at cross-sectional transitions. The refinement zones are highlighted in Fig. 9.

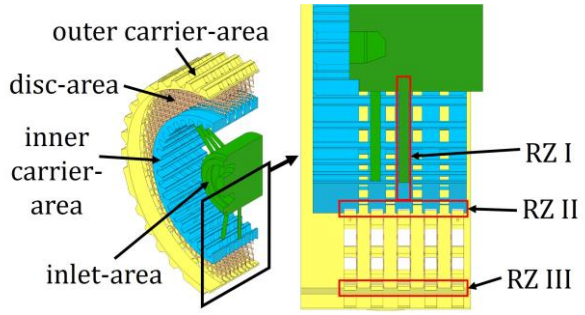

Fig. 9. Refinement zones in the calculation domain.

The mesh-study is performed for static operations. All simulations are repeated on each mesh-type with exactly the same solver settings, boundary and initialization conditions. The mesh independence of the oil flow rate through the groove gaps and the axial force due to oil pressure in the grooves are considered as convergence criteria.

Fig. 10 compares the calculated specific oil flow through the groove gaps for each mesh-type. The results seem to be independent of mesh resolution for the studied configurations.

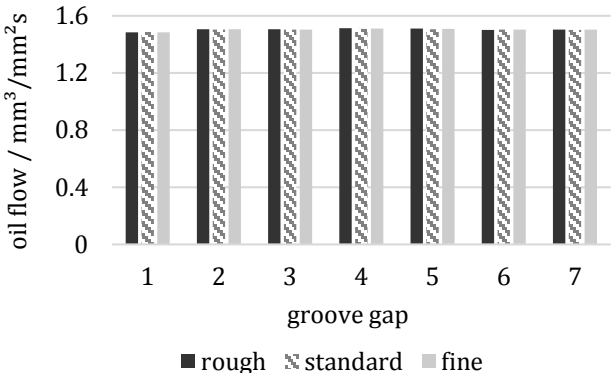

Fig. 10. Comparison of oil flow through groove gaps depending on mesh-type (variant I, L-301, ϑ_{oil} = 40 °C, static operation ST3).

Fig. 11 compares the arithmetic mean of the axial force due to oil pressure in the grooves depending on mesh type. A mesh independent solution is achieved with the standard mesh.

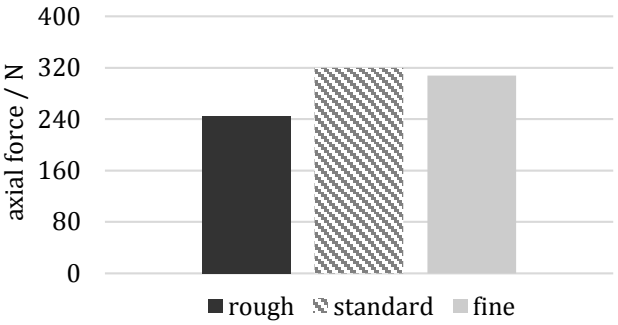

Fig. 11. Comparison of axial forces due to oil pressure in the grooves depending on mesh type (variant I, L-301, ϑ_{oil} = 40 °C, static operation ST3).

As our results show, the standard mesh seems to be the optimal compromise between solution accuracy and computational effort and is therefore used for all further calculations.

Based on the results of the mesh study, we executed a time-step-study for the dynamic operating points. As proposed in other publications, the time step is defined in terms of a fixed angular rotation (e.g. [11]). We compared the results according to our method in the mesh study by varying the time step between an angular rotation of 1 ° and 2 °. The difference in the results is smaller than 2 %, but calculation times can be nearly halved by using the time step based on a rotation of 2 °. All dynamic simulations are therefore set up to rotate 2° per time step.

The simulations are initialized with oil temperature (representing viscosity / density) and rotational speed of the plates according to the conditions in the test rig.

Static cases are initialized with the data recorded during the experimental investigations.

To adequately fulfill the assumption of an isothermal flow during constant slip operation, the representative isothermal oil temperature must be estimated. We see from the results of the static cases that the transition of the oil flow from the inner carrier-area to the grooves has the highest hydraulic resistance due to the shrinking of the cross section area. That is why we assume that this region dominates the development of the flow field. We initialize the dynamic simulations with the oil

temperature at the inner radius of the friction plates. This temperature is calculated with the thermal clutch design tool KUPSIM [5, 36].

Table 9 summarizes the oil temperatures obtained from measurements for the static cases and Table 10 summarizes the oil temperatures from KUPSIM for the dynamic cases.

Table 9. Nominal and measured oil temperatures for static cases.

	Nominal oil temperature / °C	Measured oil temperature / °C
ST1	40	37
	60	56
ST2	40	38
	60	56
ST3	40	38
	60	57
ST4	40	38
	60	57

Table 10. Oil temperatures from KUPSIM for dynamic cases.

	Specific flow rate / mm^3/mm^2s	Oil temperature (KUPSIM) / °C
LS1	0.75	81
	1.5	68
	2.5	67
LS2	0.75	103
	1.5	78
	2.5	75
LS3	0.75	119
	1.5	88
	2.5	83
LS4	0.75	137
	1.5	96
	2.5	91

Since LS5 … 6 have no test rig data (numerical study), we initialize these calculations with the temperatures from LS4.

To analyze axial oil distribution per friction interface, we evaluate the oil flow rate at each friction interface. The flow rate is then normalized by the specific flow rate to enable the assessment of uniform or non-uniform axial oil distribution (e.g. Fig. 14, Fig. 15).

We assume that pressurized oil feeding lowers the axial force at the friction interfaces and therefore also lowers torque transfer capability.

Fig. 12 shows a schematic representation of the force ratios in the clutch package. Due to pressurized oil feeding, a static oil pressure in the groove gaps (gg) between separator and friction plates builds up and generates axial forces. In the central section of the clutch package (fp 1 …4 and sp 2 … 4), these forces cancel each other out. The forces acting on sp1 and sp5 reduce the nominal contact force (dashed) and the result is the reduced contact force F_{red}.

We calculate the reduced contact force through the oil pressure in the grooves ($F_{red/g}$) acc. to formula (6) by the difference of the applied nominal force F_{nom} and the sum of the axial forces in the grooves at each friction interface ($F_{ax/gi}$).

$$F_{red/g} = F_{nom} - \sum F_{ax/g_i} \tag{6}$$

Subsequently, the reduced contact force $F_{red/g}$ is scaled with the ratio of gross friction surface (A) and grooved area ($A_{grooves}$) acc. to formula (7).

$$F_{red} = F_{red/g} \cdot \frac{A}{A_{grooves}} \tag{7}$$

Thus, we assume that the calculated pressure in the grooved area approximates the pressure in the tribological contact at the non-grooved sections of the friction interfaces.

The reduced nominal surface pressure in the clutch is then calculated by dividing the resulting contact force (F_{red}) by the gross friction surface area (A).

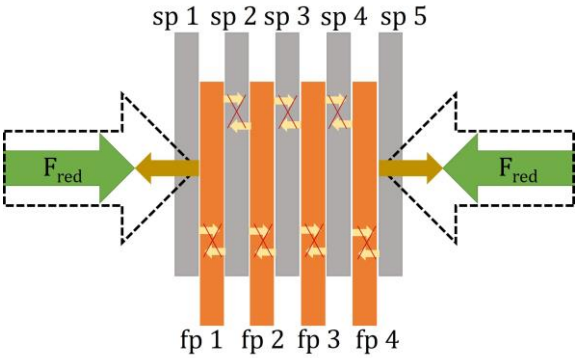

Fig. 12. Schematic representation of the force ratios in the clutch package.

2.3. Validation of CFD Approach

The numerical model is validated by comparing the calculated pressure in the inlet region with pressure measurements. Fig. 13 shows the increase of oil pressure with rising oil flow rate in both simulation and measurements. The simulation results are consistently lower than measurement data. The difference is within 10%. The same trend, with comparable relative differences, can be observed for the other static operating points.

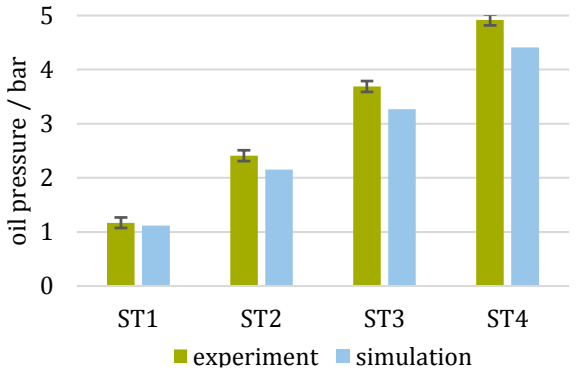

Fig. 13. Comparison of oil pressure in the inner carrier region between simulation and measurement data (variant I, L-301, ϑ_{oil} = 40 °C, static operations).

In dynamic operations, the pressure likewise increases with rising oil flow rate and the simulation results are consistently calculated lower compared to data from the test rig.

In addition, compared to static cases, the overall pressure level is reduced as rotational speed increases. Most likely the cause is a combination of lower oil viscosity in the grooves due to heating during sliding operation and the support of oil transport due to centrifugal forces.

The comparison between numerical and experimental results is challenging due to the numerical results strong dependence on reliable input parameters (a.o. [17, 31]). Since our calculation domain is based on the nominal geometry of the technical drawings, we do not expect a perfect match between simulation results and measurement data. Differences can be associated with, e.g., deviations of the groove geometry due to manufacturing processes, uncertainty in the measurements that define input parameters, and the simplifications of the flow problem.

Regardless of these circumstances, the validation showed that the simulation model can reproduce the trend and values of the measurement data accurately.

3. RESULTS AND DISCUSSION

3.1. Oil Distribution

Fig. 14 pictures the oil distribution at each friction interface for the static cases. There is only a marginal difference of supplied oil between the friction interfaces. The external groove gaps are fed with slightly less lubricant. Apparently, the position of the oil distributor that directly supplies oil to the inner friction interfaces is the cause. Hence the lubricant reaches the groove gaps of the outer friction interfaces only by axial oil flow through the inner carrier-area. However, since the maximum difference of total oil flow at each friction interface is within 0.5…1%, the classification of uniform oil distribution in the static cases seems appropriate.

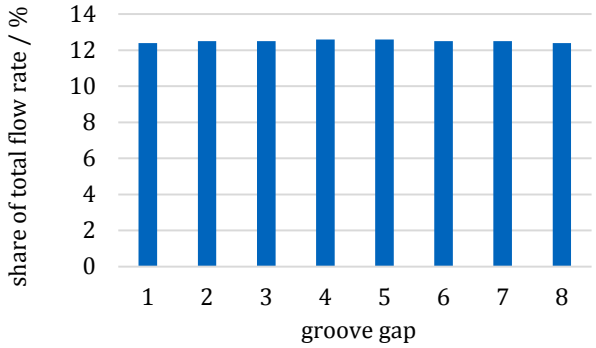

Fig. 14. Share of total flow rate at each groove gap (variant I, L-301, ϑ_{oil} = 40 °C, static operation ST3).

Fig. 15 compares the share of total flow rate at each friction interface at three different load stages in dynamic operations. There is a slightly non-uniform distribution if the ratio of the rotational speed of steel and friction plates is greater than zero. The groove gaps at the first and third friction interface are supplied with a little more lubricant than the other groove gaps. However, this difference vanishes as the ratio of rotational speed becomes 1. We could not identify the reason for this behavior. We tried to attribute it to the orientation of the grooves at each friction interface, the slightly asymmetric positioning of the oil distribution holes in the inner carrier, and the sharp edges of the steel plates by repeating simulations with optimal geometries - but the simulation results did not change.

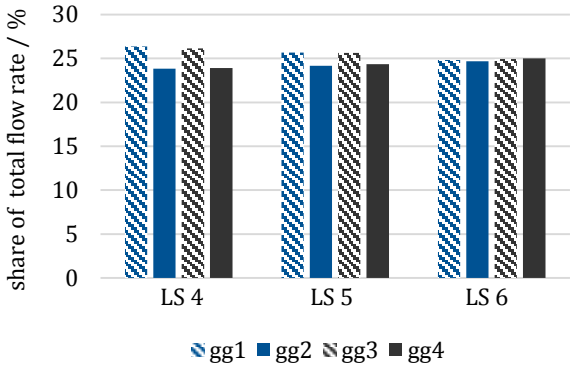

Fig. 15. Share of total flow rate at each groove gap (gg 1… 4) (variant I, L-301, dynamic operation, $\dot{v}_{spez}$ = 2.5 mm³/mm²s).

Nevertheless, since the differences are within 2%, we also conclude a nearly uniform oil distribution in the dynamic simulations.

3.2. Reduction of Axial Force

Fig. 16 (static operation) and Fig. 17 (dynamic operation) visualize the pressure distributions of the complete calculation domain. The pressure in the static case (Fig. 16) has a nearly constant value in the inlet and outlet regions. In the groove gaps, the pressure drops linearly from the inlet to outlet pressure value. The significant reduction of hydraulic cross-section between the inlet/outlet regions and the groove gaps seems to be the cause.

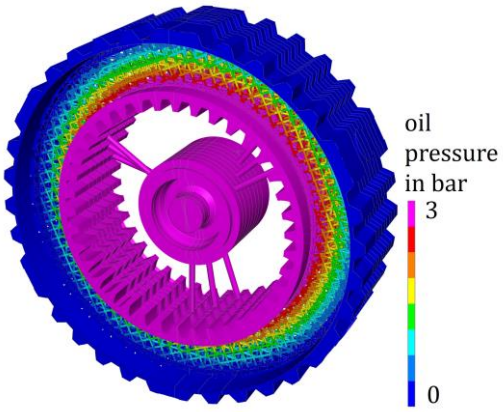

Fig. 16. Pressure distribution (variant I, L-301, ϑ_{oil} = 40 °C, static operation ST3).

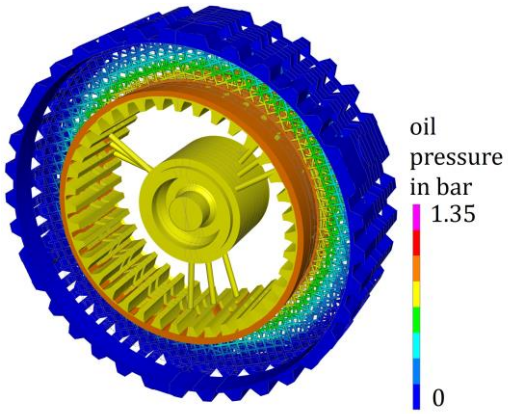

Fig. 17. Pressure distribution (variant I, L-301, dynamic operation LS3, $\dot{v}_{spez}$ = 2.5 mm³/mm²s).

In the dynamic cases at lower sliding velocities (2.5 … 5 m/s), qualitative pressure distribution is the same as in the static cases. The absolute pressure values are lower than in the static cases, most likely due to the reduction of hydraulic resistance due to the centrifugal forces.

At higher sliding velocities (7.5 … 10 m/s) the pressure distribution looks slightly different. Fig. 17 shows an example of pressure distribution in the complete calculation domain for a sliding velocity of 7.5 m/s. The pressure in the inner area slightly increases up to the transition from the inner carrier- to the groove-region, and then decreases linearly with increasing diameter according to the other cases (static / lower velocities).

The small increase in pressure in the inner carrier region seems to be caused by the isothermal modeling approach. Due to the lower fluid viscosity in combination with the centrifugal forces due to increased sliding velocities, the hydraulic resistance of the oil distributor seems to be significantly reduced. This leads to increased lubricant velocities in the spline zone of the inner carrier-area, but due to the reduction in cross-section at the transition to the grooves, the flow is blocked and thus the pressure rises.

From the pressure distribution, we calculate the reduced nominal surface pressure in the clutch package (see 2.10).

Fig. 18 compares nominal and reduced surface pressures for the static operating points. An increase of oil flow leads to higher pressure in the groove gaps, and thus reduces axial force at the friction interfaces and nominal surface pressure due to the oil flow. For static operations, the nominal surface pressure is reduced in the range of 3 … 23%.

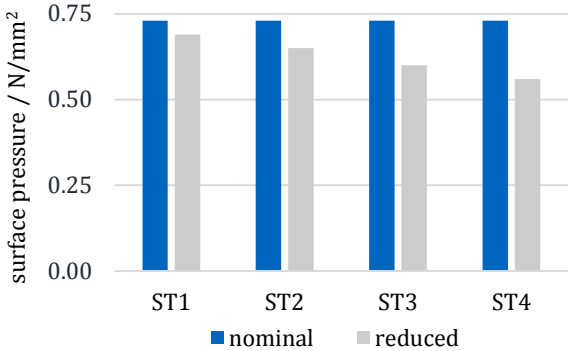

Fig. 18. Comparison of nominal and reduced surface pressures (variant I, L-301, ϑ_{oil} = 40 °C, static operation).

Fig. 19 shows the results during dynamic operations. A decreasing sliding velocity leads to an increase of hydraulic pressure, due to the oil flow reducing the axial force. The reduction of the nominal pressure for dynamic operations is as high as 29%.

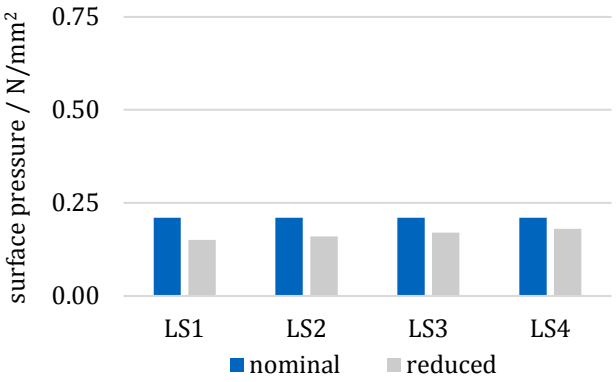

Fig. 19. Comparison of nominal and reduced surface pressure (variant I, L-301, dynamic operation, $\dot{v}_{spez}$ = 2.5 mm³/mm²s).

3.3. Geometry Variants Inner Carrier

Fig. 20 compares the oil distribution at each friction interface for variant I and variant II of the oil distributor pattern in the inner carrier during static operations. The variation in oil distributor patterns seems to not influence the oil supply to each friction interface.

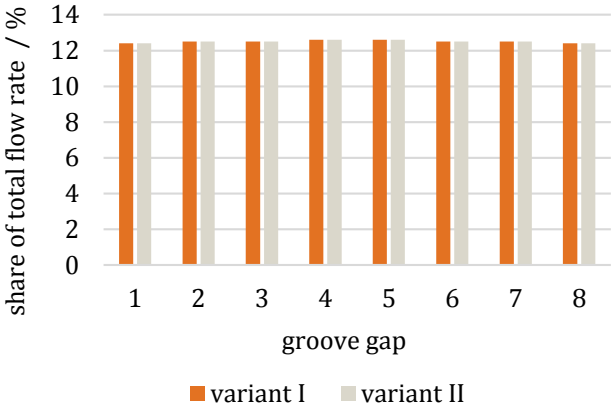

Fig. 20. Share of total flow rate at each groove gap with variations in oil distributor patterns (L-301, ϑ_{oil} = 40 °C, static operation ST3) .

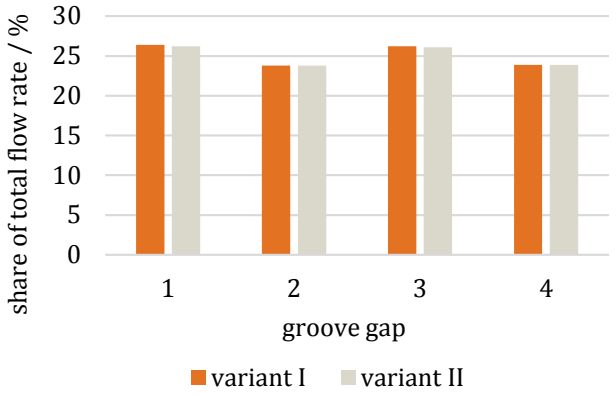

Fig. 21. Share of total flow rate at each groove gap with variations in oil distributor patterns (L-301, $\dot{v}_{spez}$ = 2.5 mm³/mm²s, dynamic operation LS4).

The same can be observed for the dynamic cases, as Fig. 21 shows. There seems to be no difference in the oil supply, despite the reduction of the radial holes in the inner carrier.

For the sake of completeness, Fig. 22 and Fig. 23 show the comparison of the reduced surface pressure under variation of the oil distributor pattern. Since the supplied oil at each friction interface is nearly the same in both cases, there is also no difference in the reduction of the nominal surface pressure.

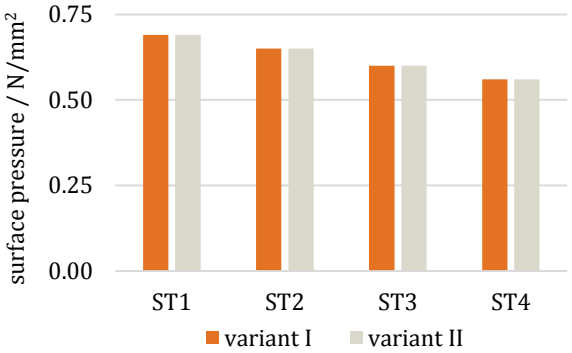

Fig. 22. Comparison of reduced surface pressure with variations in oil distributor patterns (L-301, ϑ_{oil} = 40 °C, static operation).

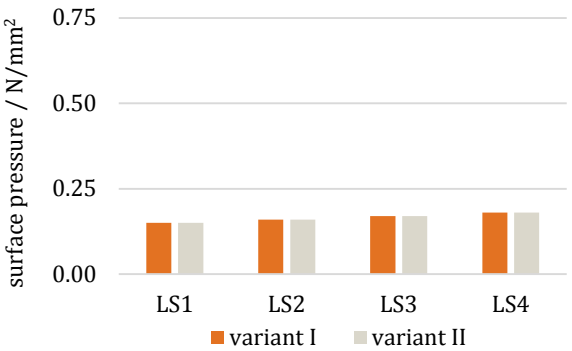

Fig. 23. Comparison of reduced surface pressure with variations in oil distributor patterns (L-301, $\dot{v}_{spez}$ = 2.5 mm³/mm²s, dynamic operation).

These results are different from published studies of automotive/motorcycle clutches, where the authors state that the oil distributor pattern of the oil supply is the main cause for differences in the oil supply at each friction interface [11, 14].

Since the clutch design in our study is sealed, we can therefore calculate a single-phase flow problem - the flow behaves like a hydraulic flow. Therefore, as long as the value of supplied oil and operating conditions such as rotational speed are constant, oil distribution seems to be independent of oil supply patterns.

4. CONCLUSION

The objective of our studies was the investigation of the oil and pressure distribution within a sealed industrial wet clutch with pressurized oil supply. Therefore, the calculation domain was extracted from a CAD model of an industrial clutch from a serial production setup in the ZF / FZG KLP-260 wet brake component test rig.

The flow is modeled as transient, laminar, incompressible, and isothermal. For mesh independent solutions of the body-fitted binary tree mesh, mesh and time step studies were carried out. A relative maximum cell size of 0.005 and a mesh rotation of 2° per time step seems to be an optimal trade-off in terms of computational effort and quality of results.

The oil temperature at the inner friction radius is used to initialize the model. In static operation, the initialization of the isothermal oil temperature is based on measurement data, whereas during dynamic operations these temperatures are determined by prior calculations.

For validation, the calculated oil pressures in the inner carrier of the numerical simulations were compared with test rig data. The simulation results are consistently underestimating (approx. 10%) the measurement data. Nevertheless, since comparisons between numerical and experimental results always seem to be challenging due to differences between simulations and experiments, the validation showed that the CFD model is capable of reproducing variations in flow rate (static) and rotational speed (dynamic) in good agreement with the test rig data.

The results of our investigations shows, that in static operations, the outer friction interfaces seem to be supplied with slightly less oil than friction interfaces in the middle of the clutch package. During dynamic operations, we also identified minor variations as long as the ratio of rotational speeds between the steel and friction plates is less than 1.

We could not identify an influence of oil distributor on the oil supply to each friction interface for the investigated pressurized clutch design. There seems to be nearly no change when the oil distributor patterns in the inner carrier are varied. The oil distribution to the individual friction interfaces and the reduction of the nominal surface pressure in static and dynamic operations does not change.

The isothermal modeling approach during dynamic operations might facilitate the negligible influence of the oil distributor design on our simulation results. The reduction of oil supply bores could lead to more non-uniform temperature distributions in the inner carrier and because of that also in the grooves. Thus, the modeling approach should be critically questioned and should be proofed in further studies by, e.g., integrating thermal calculations into the CFD simulations, although this may significantly increase computational costs.

Pressurized oil feeding significantly reduces nominal clutch pressure and therefore, acc. to formula (1), torque transfer capacity. The results show a reduction of nominal pressure (torque) up to 23 / 29 % during static / dynamic operations. However, due to the isothermal modeling approach, these results could be overestimated.

The main results of our research can be summarized as:

- Oil distribution in a sealed industrial clutch design is uniform as long as sufficient oil is supplied to ensure single-phase flow conditions.
- Axial force due to static oil pressure can significantly reduce the nominal clutch pressure, and therefore the torque transmitting capacity of the clutch.
- Axial force due to static oil pressure can be reduced by increasing rotational speed / oil temperature and by reducing oil flow rate (design optimization possible).
- The CFD approach should be further improved by incorporating effects of thermal calculations and friction material porosity during dynamic operations.

Acknowledgement

The authors gratefully acknowledge the Leibniz Supercomputing Centre for funding this project by providing computing time and support on its Linux-Cluster.

The presented results were based on research project FVA no. 413/IV, which was financed by the Research Association for Drive Technology e.V. (FVA). The authors are thankful for the sponsorship and support received from the FVA and the members of the project committee.

REFERENCES

[1] M. Hensel, *Thermal Capacity and Lifetime Behavior of Wet Multi-Plate Clutches*, PhD thesis, Gear Research Centre (FZG), Technical University of Munich, Munich, 2014. (in German)

[2] N. Lingesten, P. Marklund, E. Höglund, *The influence of repeated high-energy engagements on the permeability of a paper-based wet clutch friction material,* Proceedings of the Institution of Mechanical Engineers, Part J: Journal of Engineering Tribology, vol. 231, iss. 12, pp. 1574–1582, 2017, doi: 10.1177/1350650117700807

[3] T. Schneider, A. B. Bedrikow, K. Völkel, H. Pflaum, K. Stahl, *Comparison of Various Wet-Running Multi-Plate Clutches with Paper Friction Lining with Regard to Spontaneous Damage Behavior,* Tribology in Industry, vol. 43, no. 1, pp. 40–56, 2021, doi: 10.24874/ti.992.10.20.01

[4] G. Chen, K. Baldwin, E. Czarnecki, *Real Time Virtual Temperature Sensor for Transmission Clutches,* SAE International Journal of Engines, vol. 4, iss. 1, pp. 1523–1535, 2011, doi: 10.4271/2011-01-1230

[5] F. Wohlleber, H. Pflaum, B.-R. Höhn, *FVA No. 150/VI - Issue 899 - Final report: Software Extension for the Thermal Calculation of Multi-Plate Clutches and Integration of the Software into the FVA-Workbench,* Frankfurt/Main: Forschungsvereinigung Antriebstechnik e.V., 2009. (in German)

[6] K. Voelkel, H. Pflaum, K. Stahl, *FVA No. 150/VII - Issue 1204 - Final report: Extension of the Simulation Methodology for the Calculation of the Transient Temperature Behavior of Wet Multi-Plate Clutches,* Frankfurt/Main: Forschungsvereinigung Antriebstechnik e.V., 2016. (in German)

[7] D. Groetsch, K. Voelkel, H. Pflaum, K. Stahl, *Real-Time Temperature Calculation and Temperature Prediction of Wet Multi-Plate Clutches, preprint,* Forschung im Ingenieurwesen, 2021, doi: 10.1007/s10010-021-00529-z

[8] P. Marklund, F. Sahlin, R. Larsson, *Modelling and simulation of thermal effects in wet clutches operating under boundary lubrication conditions,* Proceedings of the Institution of Mechanical Engineers, Part J: Journal of Engineering Tribology, vol. 223, iss. 8, pp. 1129–1141, 2009, doi: 10.1243/13506501JET563

[9] J. Cui, C. Wang, F. Xie, R. Xuan, G. Shen, *Numerical investigation on transient thermal behavior of multidisk friction pairs in hydro-viscous drive,* Applied Thermal Engineering, vol. 67, iss. 1-2, pp. 409–422, 2014, doi: 10.1016/j.applthermaleng.2014.03.054

[10] M. Behzad, V. Saxena, M. Schaefer, *Thermal-Hydrodynamic Optimization of Grooves in a Wet Clutch,* in Dritev - Drivetrain for vehicles, EDrive, Transmissions in mobile machines, 27-28 June 2018, VDI-reports no. 2328, Bonn, The Association of German Engineers (VDI), pp. 101–117, doi: 10.51202/9783181023280-I-101

[11] S. Terzi, B. Manhartsgruber, M. Milani, L. Montorsi, *Optimization of the Lubrication Distribution in Multi Plate Wet-Clutches for HVT Transmissions: An Experimental - Numerical Approach,* in International Powertrains, Fuels & Lubricants Meeting, 17 September, 2018, SAE Technical Paper Series, pp. 1–11, doi: 10.4271/2018-01-1822

[12] A. Bassi, M. Milani, L. Montorsi, S. Terzi, *Dynamic Analysis of the Lubrication in a Wet Clutch of a Hydromechanical Variable Transmission,* SAE International Journal of Commercial Vehicles, vol. 9, iss. 2, pp. 280–290, 2016, doi: 10.4271/2016-01-8099

[13] A. Albers, J. Bernhardt, *Wet-running multi-plate clutches - potentials of engineering ceramic materials,* Tribologie und Schmierungstechnik, vol. 59, no. 2, pp. 15–17, 2012. (in German)

[14] C. Grünzweig, M. Wagner, J. Ruf, D. Helmer, *Visualization of Oil Distribution in a Wet Multi-Plate Clutch,* ATZ - Automobiltechnische Zeitschrift, vol. 2013, iss. 3, 224-230, 2013, (in German), doi: 10.1007/s35148-013-0061-z,

[15] W. Bin, H. yongyong, W. Wei, L. Jianbin, *Simulation and experiment of viscous torque for disengaged wet clutches of tracked vehicle,* Proceedings of the Institution of Mechanical Engineers, Part J: Journal of Engineering Tribology, vol. 233, iss. 4, pp. 593–604, 2019, doi: 10.1177/1350650118788143

[16] T. Neupert, D. Bartel, *High-resolution 3D CFD multiphase simulation of the flow and the drag torque of wet clutch discs considering free surfaces,* Tribology International, vol. 129, pp. 283–296, 2019, doi: 10.1016/j.triboint.2018.08.031

[17] R. Niedenthal, D. Groetsch, K. Voelkel, H. Pflaum, K. Stahl, *Volume of Fluid vs. Cavitation CFD-Models to Calculate Drag Torque in Multi-Plate Clutches,* in WCX SAE World Congress Experience, 21 April, 2020, SAE Technical Paper Series, pp. 1–9, doi: 10.4271/2020-01-0495

[18] P. Payvar, *Laminar heat transfer in the oil groove of a wet clutch,* International Journal of Heat and Mass Transfer, vol. 34, iss. 7, pp. 1791–1798, 1991, doi: 10.1016/0017-9310(91)90154-7

[19] A. Albers, F. Brezger, C. Koch, *Development of a new validation environment for CFD simulations on the example of a lubricated clutch,* in Drivetrain for vehicles 2012, 19-20 June 2012, VDI-reports no. 2158, Friedrichshafen, The Association of German Engineers (VDI), pp. 443–459.

[20] N. Weber, T. Skubacz, G. Poll, J. Fahl, T. Elfrath, *Fluorescence-based Investigations into the Contact of Wet-Disc Clutches. Optical investigations into the flat friction contact of multi-disc clutches,* in Drivetrain for vehicles 2010, 22-23 June 2010, VDI-reports no. 2081, Friedrichshafen, The Association of German Engineers (VDI), pp. 431–442.

[21] G. J. Meingaßner, H. Pflaum, K. Stahl, *Test-Rig Based Evaluation of Performance Data of Wet Disk Clutches,* in CTI Symposium, 30 November - 1 December, 2015, Berlin, pp. 1–11.

[22] U. Stockinger, D. Groetsch, F. Reiner, K. Voelkel, H. Pflaum, K. Stahl, *Friction behavior of innovative carbon friction linings for wet multi-plate clutches,* Forschung im Ingenieurwesen, vol. 85, iss. 1, pp. 115–127, 2021, doi: 10.1007/s10010-020-00436-9

[23] A. Baumgartner, *Friction Behavior of Wet Disk Clutches - Uncertainty of Measurement and Evaluation Methods*, Master Thesis, Gear Research Centre (FZG), Technical University of Munich, Munich, 2020. (in German)

[24] JCGM 100:2008, *Evaluation of measurement data - Guide to the expression of uncertainty in measurement*, 2008.

[25] DIN EN ISO 14253-2, *Geometrical product specifications (GPS) - Inspection by measurement of workpieces and measuring equipment - Part 2: Guidance for the estimation of uncertainty in GPS measurement, in calibration of measuring equipment and in product verification*, 2018.

[26] W. Polifke, J. Kopitz, *Heat transfer, fundamentals, analytical and numerical methods,* München: Pearson Studium, 2009. (in German)

[27] DIN 51757, *Testing of mineral oils and related materials – Determination of density.*

[28] DIN 51563, *Testing of Mineral Oils and Related Materials – Determination of Viscosity Temperature Relation – Slope m.*

[29] K. Voelkel, *Characterization of the Running-In Behavior of Wet Multi-Plate Clutches*, PhD thesis, Gear Research Centre (FZG), Technical University of Munich, Munich, 2020. (in German)

[30] Simerics Inc., *Simerics MP+ Manual v5.1,* Seattle: Simerics Inc., 2020.

[31] P. Payvar, Y. N. Lee, W. J. Minkowycz, *Simulation of heat transfer to flow in radial grooves of friction pairs,* International Journal of Heat and Mass Transfer, vol. 37, iss. 2, pp. 313–319, 1994, doi: 10.1016/0017-9310(94)90102-3

[32] F. Pfleger, *Shifting and lifetime behavior of multiplate clutches*, PhD thesis, Gear Research Centre (FZG), Technical University of Munich, Munich, 1998. (in German)

[33] B. Haemmerl, *Lifetime and Temperature Behavior of Oil-Cooled Multi-plate Clutches under Load Collective Stresses*, PhD thesis, Gear Research Centre (FZG), Technical University of Munich, Munich, 1995. (in German)

[34] F. Wohlleber, *Thermal Behavior of Wet Multi-Plate Clutches*, PhD thesis, Gear Research Centre (FZG), Technical University of Munich, Munich, 2012. (in German)

[35] H. Ding, F. C. Visser, Y. Jiang, M. Furmanczyk, *Demonstration and Validation of a 3D CFD Simulation Tool Predicting Pump Performance and Cavitation for Industrial Applications,* Journal of Fluids Engineering, vol. 133, iss. 1, p 273, 2011, doi: 10.1115/1.4003196

[36] K. Voelkel, H. Pflaum, K. Stahl, 2016, *Das thermische Verhalten nasslaufender Lamellenkupplungen - Simulation mit dem FVA-Programm KUPSIM*, in Forschungsvereinigung Antriebstechnik (ed) Getlub - Tribologie- und Schmierstoffkongress, vol. 2016, Würzburg, pp. 86–96. (in German)